Supplementary Information for

Surface Lattice Oxygen-Promoted ZnO Catalyst for Ethanol Nonoxidative Dehydrogenation

Zheng Zhang[a, d, 1], Mingming Hou[a, c, d, 1], Tao Gan[b], Wenjuan Zhang[a, d], Gang Liu[a, d, *]

[a] *State Key Laboratory of Inorganic Synthesis and Preparative Chemistry, College of Chemistry, Jilin University, Changchun, 130012, China*

[b] *Shanghai Synchrotron Radiation Facility, Shanghai Advanced Research Institute, Chinese Academy of Sciences, Shanghai, China*

[c] *Hubei Key Laboratory of Energy Storage and Power Battery, School of Mathematics, Physics and Optoelectronic Engineering, Hubei University of Automotive Technology, Shiyan, 442002, China.*

[d] *Key Laboratory of Surface and Interface Chemistry of Jilin Province, College of Chemistry, Jilin University, Changchun, 130021, China*

* Corresponding authors: lgang@jlu.edu.cn (Gang Liu).

[1] The authors have contributed equally to this work.

Supplementary Methods

1. Catalyst Preparation

Synthesis of ZrO_2 catalyst. The ZrO_2 catalyst as shown in Fig.1b was synthesized using a precipitation method, with modifications inspired by previously reported procedures[1]. In this process, 12.88 g of zirconium nitrate pentahydrate was dissolved in 50 mL of distilled water to prepare a 0.6 mol L^{-1} solution at 70 °C. A 0.75 mol L^{-1} sodium carbonate solution was then introduced dropwise as a precipitating agent while the pH was adjusted to 7 under continuous stirring. The resulting suspension was aged at 70 °C for 3 hours with agitation, followed by filtration. The collected precipitate was dried at 100 °C for 8 hours and subsequently calcined in a muffle furnace at 500 °C for 3 hours to yield the final catalyst.

Synthesis of spiciform ZnO catalyst. The spiciform ZnO catalyst was synthesized using a hydrothermal method[2]. 1.37 g of Zinc chloride and 1.53 g of ammonium carbonate were dissolved in 40 mL of deionized water to form a solution. The resulting mixture was transferred to a 100 mL Teflon-lined autoclave, sealed, and maintained at 90 °C for 3 hours. After cooling to room temperature, the white precipitate was filtered, washed several times with deionized water and anhydrous ethanol, dried at 60 °C for 3 hours, and then calcined at 400 °C for 15 minutes to yield the catalyst.

Synthesis of hexagonal needle-like ZnO catalyst. The hexagonal needle-like ZnO catalyst was prepared by a hydrothermal method[3]. 8.92 g of Zinc nitrate hexahydrate was dissolved in 60 mL of water, while 12.00 g of sodium hydroxide was dissolved in another 60 mL of water. The sodium hydroxide solution was added to the zinc nitrate solution, stirred for 30 minutes, and then transferred into a 200 mL stainless steel autoclave. The hydrothermal synthesis was conducted at 60 °C for 12 hours. After cooling to room temperature, the white solid was collected, centrifuged three times with 500 mL of deionized water, dried overnight in an 80 °C oven, and calcined at 400 °C for 2 hours to obtain the catalyst.

Synthesis of Spherical ZnO Catalyst. The nanospherical ZnO catalyst was synthesized via a coprecipitation method. Specifically, 29.75 g of Zinc nitrate hexahydrate was dissolved in 100 mL of deionized water to form a 1.0 mol L^{-1} zinc nitrate solution. A 1.0 mol L^{-1} sodium carbonate solution was added dropwise as a precipitant to adjust the pH of the mixture to 10. The mixture was aged under stirring for 3 hours, filtered, and dried at 100 °C for 12 hours. The dried product was then ground into a fine powder and calcined at 450 °C for 4 hours, denoted as ZnO (Air).

Synthesis under different surface pretreatment conditions. The primary catalyst discussed in this study, spherical ZnO (Air), was subjected to surface pretreatment at 450 °C for 1 hour under varying atmospheres, including N_2 and 10%

H_2/Ar conditions. The catalysts pretreated in H_2 and N_2 are referred to as ZnO (H_2) and ZnO (N_2), respectively.

2. Catalyst Evaluation

Catalytic performance tests were conducted in a fixed-bed reactor. Specifically, a predetermined amount of catalyst (1.0 g) was loaded into a tubular reactor. Ethanol and nitrogen (N_2) as a carrier gas were introduced from the top of the reactor. The reaction conditions were maintained at 0.1 MPa, 593 K, with the liquid ethanol flow rate of 3.6 $mL \cdot h^{-1}$ and N_2 flow rate of 20 $mL \cdot min^{-1}$. The liquid-phase products were analyzed using a gas chromatograph (GC) equipped with a flame ionization detector (FID) and an SE-54 column (30 m length, 0.25 mm internal diameter).

The calculations for ethanol conversion, acetaldehyde selectivity, and yield were as follows:

Ethanol Conversion (%) *= Moles of carbon in total products / (Moles of carbon in total products + Moles of carbon in unreacted ethanol) × 100%*

Acetaldehyde Selectivity (%) *= Moles of carbon in acetaldehyde / (Moles of carbon in total products) × 100%*

Acetaldehyde Yield (%) *= Ethanol Conversion × Acetaldehyde Selectivity*

3. Catalyst Characterization

Scanning Electron Microscopy (SEM). The samples were characterized using a SU8020 scanning electron microscope. Prior to testing, the samples were dispersed on conductive adhesive surfaces and subsequently coated with a thin layer of gold.

X-ray Powder Diffraction (XRD). XRD analysis of all samples was performed using a Rigaku X-ray diffractometer with a Cu K_α radiation source. The instrument operated at a voltage of 40 kV and a current of 40 mA. The scanning speed was set to 10°/min, covering a wide angle range from 10° to 80° for analysis.

N_2 adsorption-desorption experiment. Approximately 100 mg of the sample was accurately weighed and placed in a sample tube for adsorption-desorption measurements. The sample was vacuum-degassed at 100 °C over 12 hours to remove any moisture or contaminants, followed by an accurate mass recording post-degassing. Measurements were then taken in a liquid nitrogen bath using a Belsorp-max automated analyzer to determine surface area and pore characteristics. The adsorption-desorption isotherms were processed using both the BET (Brunauer-Emmett-Teller) method and the BJH (Barrett-Joyner-Halenda) analysis for surface parameters evaluation.

Hydrogen temperature programmed reduction (H_2-TPR). A 50 mg portion of the sample was weighed and packed into a U-shaped quartz wool-lined tube. The sample underwent pretreatment under a N_2 flow of 30 mL min^{-1} at 250 °C for an hour, then cooled to 30 °C. The gas line was subsequently switched to a 5% H_2/Ar mixture, and the temperature was increased from 30 °C to 800 °C at a rate of 10 °C min^{-1}. The

variation in hydrogen concentration during the reduction was monitored through a thermal conductivity detector (TCD) using a ChemBET Pulsar TPR analyzer.

Ultraviolet-visible spectroscopy (UV-Vis). The UV-Vis spectra were obtained with a Shimadzu-2700 spectrophotometer, using $BaSO_4$ as the reflective standard. Scans were performed within the 200-800 nm wavelength range to characterize the sample's electronic structure.

X-ray photoelectron spectroscopy (XPS). XPS measurements were carried out on a Thermo ESCA LAB 250 spectrometer, employing Al K_α (1486.6 eV) as the excitation source. Instrument calibration was achieved by referencing the adventitious carbon (C 1s) peak at 284.8 eV. Additionally, the surface Auger electrons were collected during the XPS analysis to obtain Auger electron spectra (XAES).

X-ray absorption spectroscopy (XAS). Zn K-edge XAS characterization was performed at the Shanghai Synchrotron Radiation Facility (SSRF) on the BL11B beamline, using a Si(111) monochromator. Both X-ray absorption near-edge structure (XANES) and extended X-ray absorption fine structure (EXAFS) spectra were collected to analyze valence and bonding environments. Catalysts, including H_2-treated and air-treated ZnO samples, were uniformly dispersed on adhesive tape and examined in transmission mode at room temperature.

Supplementary Figures and Tables

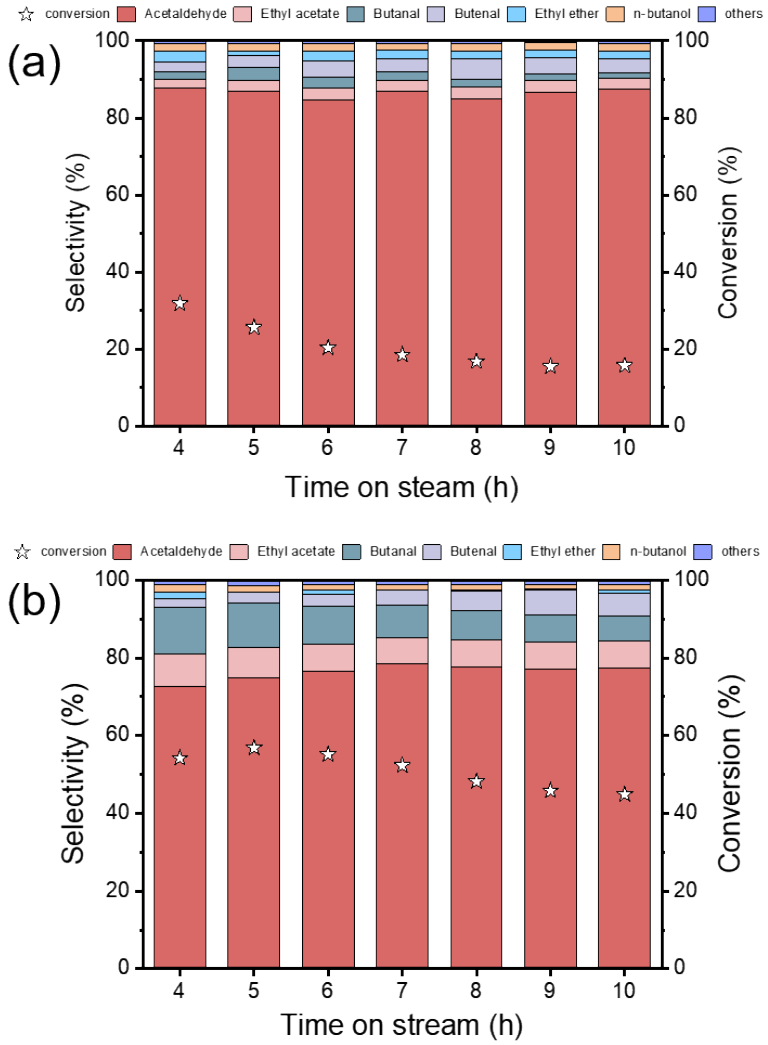

Fig. S1: Catalyst activity of ZnO with different morphologies corresponding to Figs. S3 and S4, with hexagonal needle-shaped ZnO (a) and spiciform ZnO (b) at the reaction condition: sample 1 g; 320 °C, 0.1 MPa, 20 mL min^{-1} N_2; ethanol feed 3.6 mL h^{-1}, WHSV=2.8 h^{-1}.

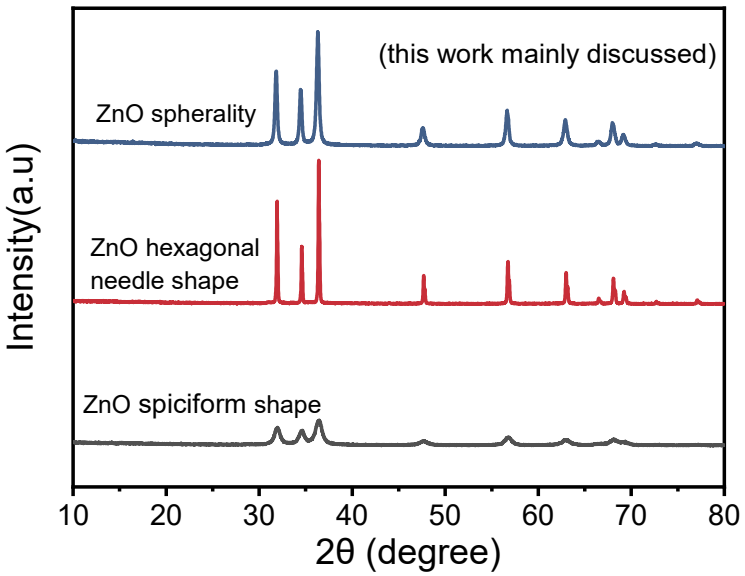

Fig. S2: XRD patterns of different morphologies of ZnO.

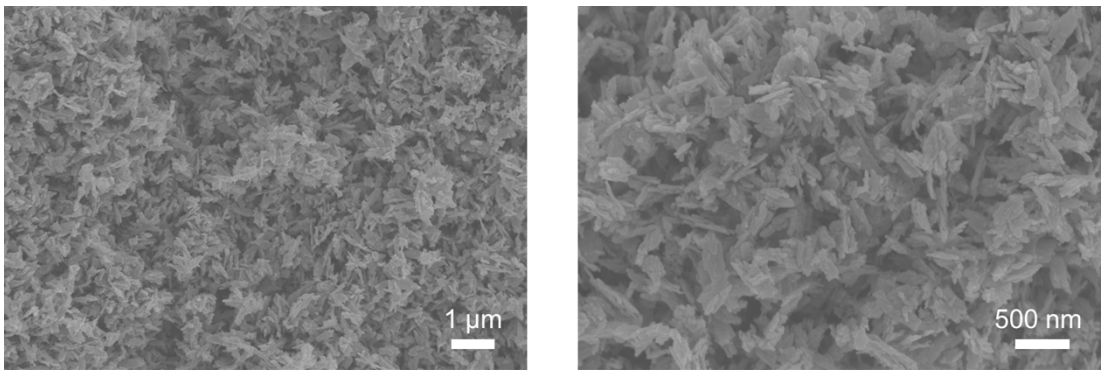

Fig. S3: SEM images of spiciform ZnO.

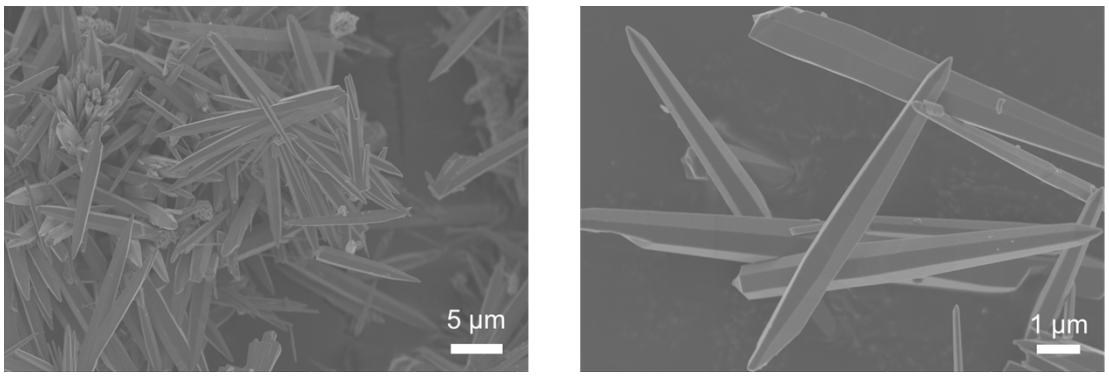

Fig. S4: SEM images of hexagonal needle shaped ZnO.

Table S1. Statistical average of the structure of the samples.

Entry	Sample	β (rad*10^5)	2θ (°)	d (nm)
1	N_2 treatment	529	36.3	28.9
2	H_2 treatment	539	36.3	28.4
3	Air treatment	568	36.3	26.9

The average crystallite size (d) of nano-sized particles can be determined by analyzing the X-ray diffraction (XRD) spectra (Figure 2d) using the Debye-Scherrer formula. The formula was expressed as follows:

$$\text{average crystallite size } d = \frac{k\lambda}{\beta cos\theta}$$

Here, k represents the Scherrer constant, which has a value of 0.94 for spherical nano-sized particles. λ denotes the wavelength of the X-ray, measured at 0.154 nm. β corresponds to the full width at half maximum (FWHM) of the strong and symmetric diffraction peak, measured in radians. θ is associated with the Bragg diffraction angle for the peak.

Notes: The ZnO catalyst exhibits excellent structural stability under reaction conditions, as shown by XRD analysis using the Scherrer formula. The crystallite sizes remain consistent before and after reactions, confirming the robustness of the structure of ZnO catalyst. While the crystallite size derived from XRD reflects an average along specific orientations, the stability trend is consistent with electron microscopy observations.

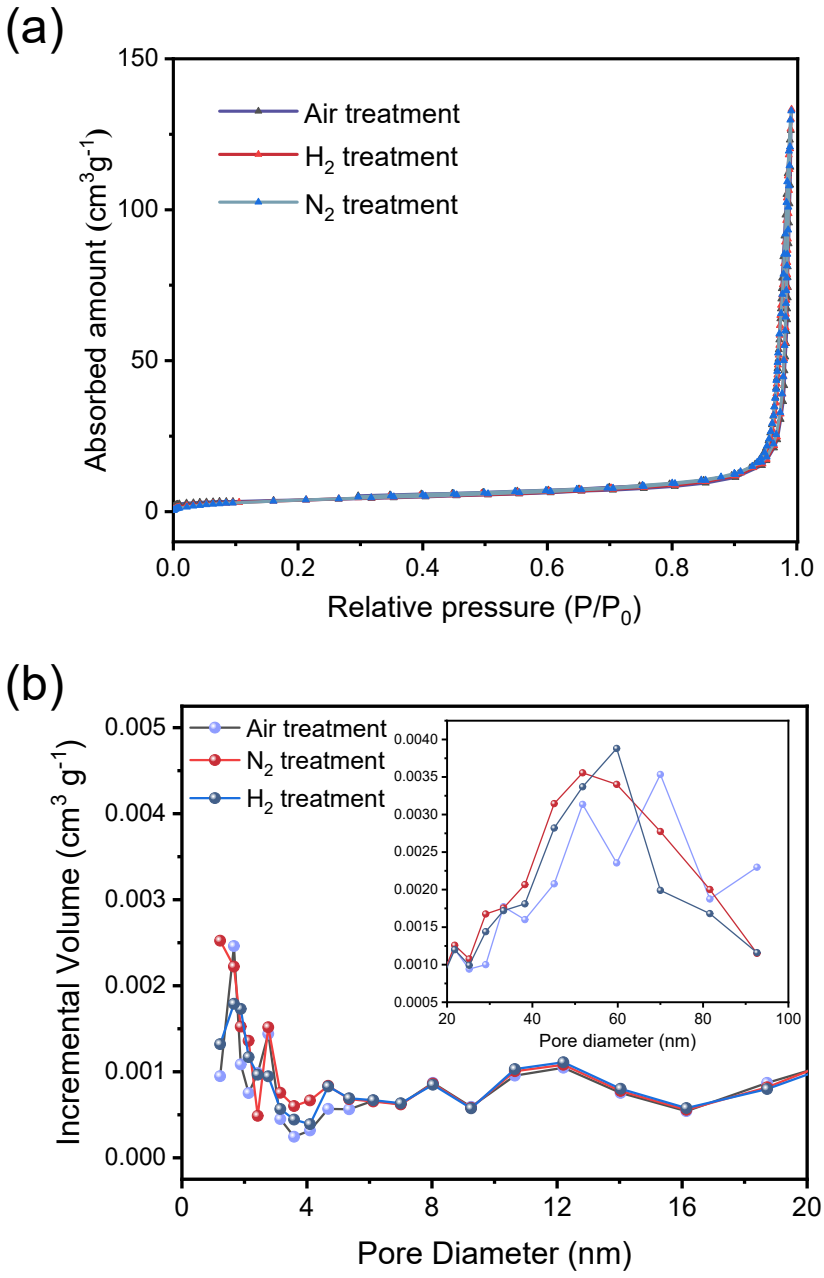

Fig. S5: (a) N_2 adsorption-desorption isotherms towards the different treated samples. (b) Pore size distribution from N_2 adsorption-desorption measurement towards the different treatments of ZnO.

Table S2. Porous properties of samples towards the different treatments of ZnO from N_2 adsorption-desorption experiment and corresponding ethanol conversion.

Catalyst	S_{BET} (m^2 g^{-1})	Mean pore size (nm)	Total pore volume (cm^3 g^{-1})	Ethanol conversion (%)
ZnO-450 °C Air	13	56.0	0.18	42.6
ZnO-450 °C N_2	13	57.2	0.20	< 10.0
ZnO-450 °C H_2	13	59.0	0.20	< 10.0

Notes: ZnO-450 °C refers to ZnO catalysts calcined at 450 °C under different atmospheres (e.g., air, N_2, or H_2).

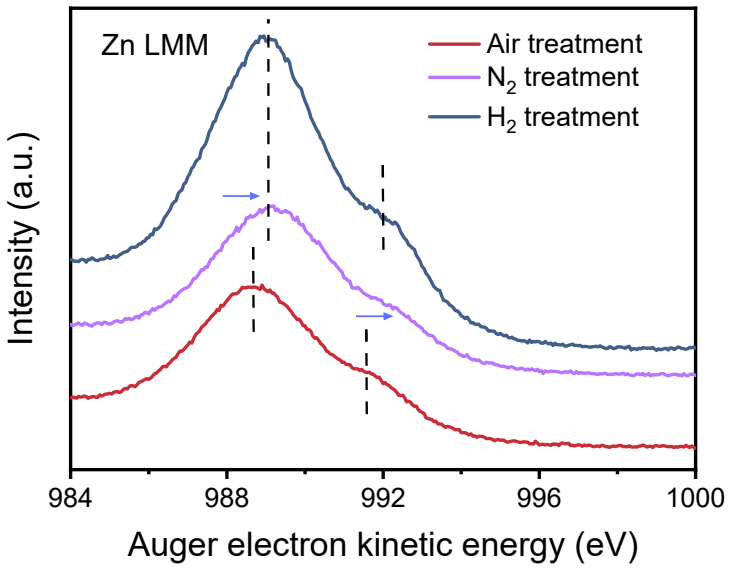

Fig. S6: Zn LMM XAES of kinetic energies from the different treatments of ZnO.

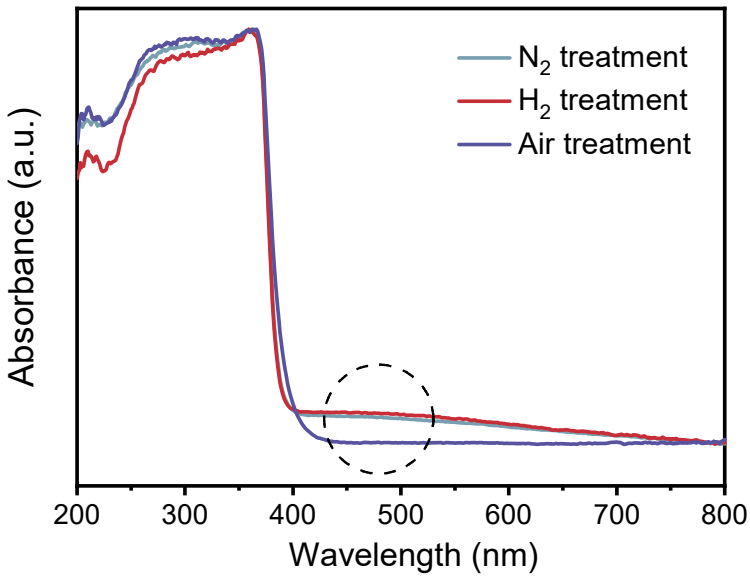

Fig. S7: UV-vis patterns of the different treatments of ZnO.

Notes: The analysis demonstrates that the treated ZnO contains a significant number of oxygen vacancies. These vacancies increase the electron density around vacancy sites, altering the local electronic environment measured by XPS analysis (Figure 3). Moreover, the rise in oxygen vacancies correlates with a reduction in surface lattice oxygen, affecting the availability of active oxygen species and thereby influencing the catalytic activity.

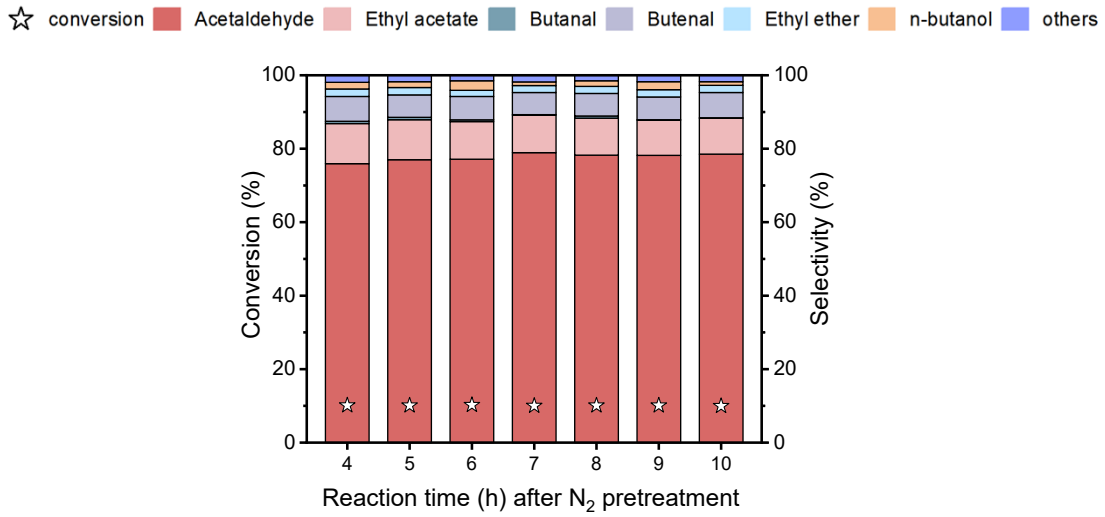

Fig. S8 Ethanol conversion and organic product distributions over ZnO in the additional pre-treatment of N_2 (b) at 450 °C for 1h. Reaction condition: sample 1 g; 320 °C, 0.1 MPa, ethanol feed 3.6 mL h^{-1}.

Notes: The decline in acetaldehyde selectivity at lower conversion rates for treated ZnO can be attributed to surface modifications induced by reaction conditions. The reduction in surface lattice oxygen and the associated increase in oxygen vacancies expose more Zn sites, altering the catalytic surface. This change makes acetaldehyde molecules more prone to further reactions, leading to the formation of by-products and a decrease in selectivity, even at lower conversion rates.

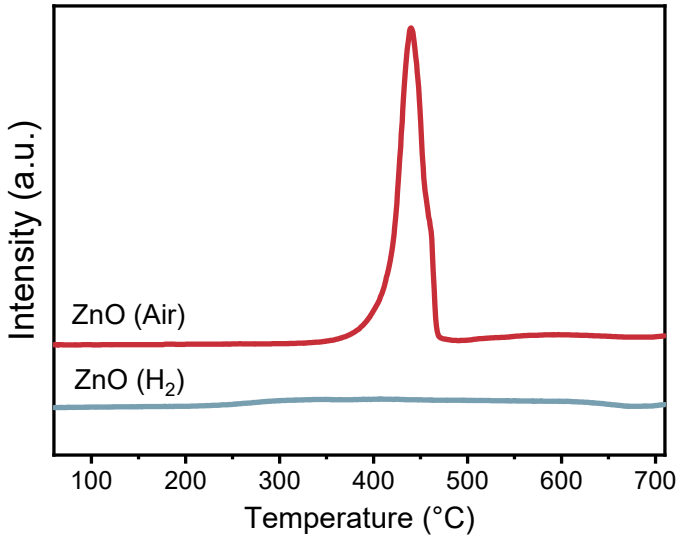

Fig. S9: H_2-TPR profiles of the ZnO catalysts for air and H_2 treatment.

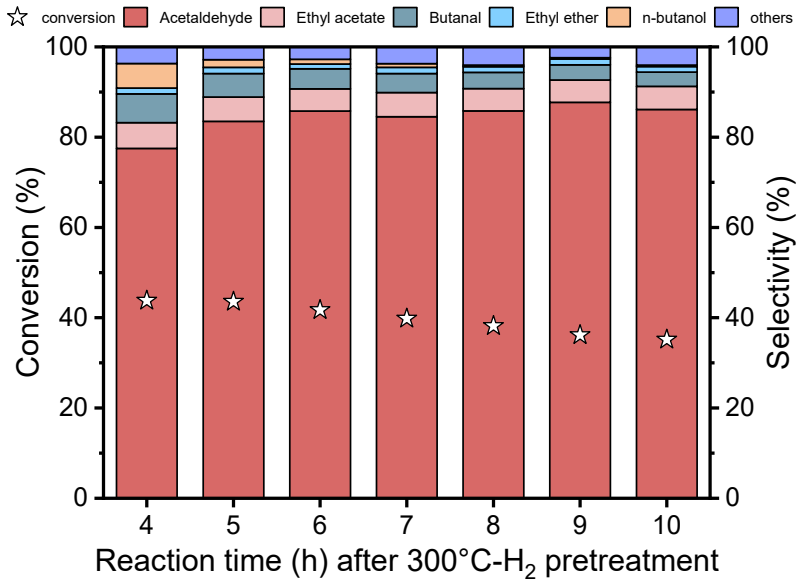

Fig. S10: Ethanol conversion and organic product distributions over as-prepared ZnO after the condition of low hydrogen reduction intensity at 300 °C for 1h.

Table S3. EXAFS fitting parameters of as-synthesized catalysts and standard sample.

Catalyst	Path	CN	Distance (Å)	σ^2 for O and Zn (10^{-3} Å^2)	δE_0 (eV)	ρ (%)
ZnO-standard	Zn-O	3.9 ± 0.6	1.965 ± 0.012	5.5 ± 1.4	2.8 ± 1.9	2.5
	Zn-Zn	5.9 ± 0.9	3.210 ± 0.011	6.0 ± 1.2		
ZnO-450 °C Air	Zn-O	1.4 ± 0.3	1.953 ± 0.009	4.7 ± 1.8	2.8 ± 1.4	1.5
	Zn-Zn	6.9 ± 1.8	3.230 ± 0.010	12.6 ± 1.4		
ZnO-450 °C H_2	Zn-O	0.4 ± 0.1	1.931 ± 0.019	4.9 ± 3.3	2.9 ± 2.9	4.5
	Zn-Zn	1.4 ± 0.7	3.210 ± 0.018	8.9 ± 2.4		

Notes: The coordination numbers derived from EXAFS fitting of Zn-O and Zn-Zn pathways reveal critical insights into the structure-activity relationship of ZnO in ethanol dehydrogenation. Standard ZnO, with fully saturated bulk lattice oxygen coordination, exhibits low catalytic activity due to the shielding of Zn active sites by saturated O, which prevents their participation in catalytic reactions. In contrast, the synthesized ZnO nanoparticles, with relatively reduced Zn-O coordination (1.4) due to the intrinsic surface defects of ZnO nanoparticles prepared by air calcination, show significantly improved activity. This improvement is attributed to the exposure of both Zn and surface lattice oxygen, which synergistically contribute to key steps in the reaction, such as ethanol activation and bond cleavage.

Under progressive reduction conditions (e.g., H_2 treatment), the Zn-O coordination number drops further to 0.4, indicating a substantial loss of surface lattice oxygen. This disrupts the critical interaction between Zn and oxygen, leading to diminished catalytic

performance despite increased Zn exposure. These findings emphasize the importance of balancing Zn exposure and lattice oxygen availability to achieve high catalytic efficiency. The synergistic interplay between Zn and surface lattice oxygen serves as the foundation for the proposed reaction mechanism and highlights the necessity of controlling surface coordination and defects in ZnO-based catalysts.

References

1. J. Wang, G. Li, Z. Li, C. Tang, Z. Feng, H. An, H. Liu, T. Liu and C. Li, *Sci. Adv.*, **3**, e1701290.
2. Y. Wan, J. Li, J. Ni, C. Wang, C. Ni and H. Chen, *J. Hazard. Mater.*, 2022, **435**, 129073.
3. T. Guo, G. Xu, S. Tan, Z. Yang, H. Bu, G. Fang, H. Hou, J. Li and L. Pan, *J. Alloys Compd.*, 2019, **804**, 503-510.